AGU PUBLICATIONS

JGR

Journal of Geophysical Research: Atmospheres

RESEARCH ARTICLE
10.1002/2017JD026959

Key Points:
- Ocean warming could lead to the eastward withdrawal of western Pacific subtropical high and thus the northward turning of tropical cyclone
- Northward turning of tropical cyclone can be attributed to the larger storm size under higher sea surface temperature condition
- The increase of storm size can be largely attributed to the feedback between surface enthalpy flux and tangential wind in the outer region

Supporting Information:
- Supporting Information S1
- Figure S1
- Figure S2
- Figure S3
- Figure S4
- Figure S5
- Figure S6
- Figure S7
- Figure S8
- Figure S9
- Data Set S1
- Data Set S2
- Data Set S3

Correspondence to:
T. Li,
timli@hawaii.edu

Citation:
Sun, Y., Z. Zhong, T. Li, L. Yi, S. J. Camargo, Y. Hu, K. Liu, H. Chen, Q. Liao, and J. Shi (2017), Impact of ocean warming on tropical cyclone track over the western north pacific: A numerical investigation based on two case studies, *J. Geophys. Res. Atmos.*, *122*, 8617–8630, doi:10.1002/2017JD026959.

Received 14 APR 2017
Accepted 9 AUG 2017
Accepted article online 14 AUG 2017
Published online 26 AUG 2017

Impact of ocean warming on tropical cyclone track over the western north pacific: A numerical investigation based on two case studies

Yuan Sun[1,2], Zhong Zhong[3,2], Tim Li[1,4], Lan Yi[5], Suzana J. Camargo[6], Yijia Hu[2], Kefeng Liu[2], Haishan Chen[1], Qianfeng Liao[2], and Jian Shi[2]

[1]Key Laboratory of Meteorological Disaster, Ministry of Education/Joint International Research Laboratory of Climate and Environmental Change/Collaborative Innovation Center on Forecast and Evaluation of Meteorological Disasters, Nanjing University of Information Science and Technology, Nanjing, China, [2]College of Meteorology and Oceanography, National University of Defense Technology, Nanjing, China, [3]Jiangsu Collaborative Innovation Center for Climate Change, School of Atmospheric Sciences, Nanjing University, Nanjing, China, [4]IPRC and Department of Atmospheric Sciences, University of Hawai'i at Mānoa, Honolulu, Hawaii, USA, [5]Chinese Academy of Meteorological Sciences/Chinese Meteorological Society, Beijing, China, [6]Lamont-Doherty Earth Observatory, Columbia University, Palisades, New York, USA

Abstract The impact of ocean warming on tropical cyclone (TC) track over the western North Pacific is an open issue. Relatively little is known about possible changes in TC tracks under ocean warming conditions due to both inhomogeneous observation networks and large natural variability over a relatively short observational period. A suite of semiidealized numerical experiments on two TC cases is conducted to investigate the response of TC tracks to increases in sea surface temperature (SST). It is found that the simulated TC track is highly sensitive to underlying SST. Specifically, through its influence on the radial distribution of sea surface enthalpy, ocean warming can lead to changes in the tangential wind profile and thus increase the TC size in terms of the radius of gale force wind, which is attributed to the increase in maximum wind speed, the expansion of the radius of maximum wind, and the additional increase in outer winds. The increased TC size, as suggested by previous studies, further leads to the eastward withdrawal of the western Pacific subtropical high (WPSH) and thus a northward turning of the TC. Results of climate simulations in the present study provide further evidence for the aforementioned impact of ocean warming on TC size and thus the WPSH and TC track. Results of the present study also imply that the threat of storms to countries in East Asia may be reduced due to possible changes in TC tracks if ocean warming continues in the future.

Plain Language Summary In this paper we investigate the impact of ocean warming on tropical cyclone (TC) track over the western North Pacific (WNP). Our model results show that as the sea surface temperature (SST) increases, the TC expands significantly amplifying the influence of TC on the surrounding environmental flow associated with the western Pacific subtropical high and eventually leading to the northward turning of TC over the WNP. Our results also implies that the threat of storm to the countries in the East Asian may reduce due to the change of TC track if ocean warming happens in future.

1. Introduction

The centennial trend of global temperature increase has been attributed to greenhouse gas increases since the industrial revolution [*Cox et al.*, 2000]. Because of the vast spatial area covered by the oceans and the strong interannual and interdecadal sea surface temperature (SST) variability found there, SST is expected to contribute significantly to the observed global warming [*Lau and Weng*, 1999]. Since low-level latent and sensible heat fluxes are important energy sources for tropical cyclones (TCs), SST is a vital factor impacting TC genesis and intensification [*Emanuel*, 1986; *Rotunno and Emanuel*, 1987; *Holland*, 1997; *Persing and Montgomery*, 2005; *Bell and Montgomery*, 2008]. Recent studies have further quantified the sensitivity of observed and modeled TC intensity to SST [*Elsner et al.*, 2012; *Strazzo et al.*, 2013, 2015]. Therefore, increases in SST in the context of global warming are expected to play an important role in determining TC activity changes [*Vecchi and Soden*, 2007; *Vecchi et al.*, 2008; *Kang and Elsner*, 2012; *Sun et al.*, 2013, 2014a; *Kang and Elsner*, 2016]. While progress has been made in assessing the impact of SST changes on TC genesis and intensity [*Knutson et al.*, 2010], relatively little is known about possible changes in TC tracks under ocean warming conditions [*Wang et al.*, 2011].

As suggested by *Kossin et al*. [2014], the average location where TCs reach their peak lifetime intensity has systematically migrated poleward in both the Northern and Southern Hemispheres over the past 30 years. The largest contribution to the Northern Hemisphere trend (53 km decade^{-1}) is from TCs in the western North Pacific (WNP), which is also the most active TC basin in the world in terms of annual TC frequency and accumulated cyclone energy [*Maue*, 2011; *Lee et al*., 2012]. The prevailing poleward shift of TCs over the WNP is generally attributed to the tropical belt expansion in the context of global warming [*Kossin et al*., 2014; *Wu et al*., 2014; *Kossin et al*., 2016], but the mechanisms involved are not well known yet.

TC motion is mainly steered by the large-scale environmental flow [*George and Gray*, 1977]. Since the western Pacific subtropical high (WPSH) is one of the most important components of the East Asian monsoon system, the WPSH-related large-scale forcing plays a crucial role in determining both the East Asian monsoon climate and TC tracks over the WNP [*Zhong*, 2006; *Sun et al*., 2014b, 2015a]. Recent studies based on numerical models indicated that both TC intensity and TC size are sensitive to changes in underlying SST [*Xu and Wang*, 2010; *Sun et al*., 2013, 2014a]. In other words, large-scale ocean warming can lead to not only TC intensification but also TC expansion. As suggested by *Sun et al*. [2015b], with an increase in TC size, the main body of the WPSH tends to withdraw eastward, and the TC tends to turn northward earlier. Meanwhile, TC motion often deviates from the large-scale environmental flow owing to the beta-effect propagation, which depends on outer wind strength and thus is highly sensitive to TC size [*Holland*, 1983; *Fiorino and Elsberry*, 1989; *Carr and Elsberry*, 1997]. In the background of climate change and economic impacts resulting from WNP TCs, it is of great societal importance to understand whether and how ocean warming may affect TC track. However, the lack of TC size observations and its large natural variability over a relatively short observational period makes it difficult to determine what percentage of the observed TC track change can be attributed to the ocean warming effect caused by greenhouse gas forcing [*Webster et al*., 2005; *Knutson et al*., 2010]. Moreover, the horizontal resolutions of existing climate simulations are not high enough to reproduce the TC eyewall evolution and TC size change.

The objective of this study is to assess the impact of ocean warming on TC track over the WNP. The present study sheds new light on this topic by conducting a suite of semiidealized high-resolution SST sensitivity experiments that eliminate the interference of natural variability. This study is focused on the physical processes involved in ocean warming impacts on TC size. To investigate the impact of ocean warming on TC track over the WNP, a suite of sensitivity experiments is designed for the cases of Typhoon Songda (2004) and Typhoon Megi (2010). The Weather Research and Forecasting (WRF) model forced by artificially changed SSTs is used to simulate the two TC cases [*Skamarock et al*., 2008]. The paper is organized as follows. Section 2 describes the model configuration and experiment design. Results of model simulations are presented in section 3. The physical mechanism is analyzed in section 4. Conclusions and discussion are given in the final section.

2. Model Configuration and Experiment Design

To assess the impact of ocean warming on TC track over the WNP, case studies of TC Songda (2004) and TC Megi (2010) are conducted in the present study. Both TCs are characterized by high-intensity, rapid development, long-duration, and a typical turning track. As both storms formed to the south of the WPSH, their movement and abrupt turning were closely related to the withdrawal/extension of the WPSH. The track information for both TCs is provided by the Joint Typhoon Warning Center (http://www.usno.navy.mil/NOOC/nmfc~ph/RSS/jtwc/best_tracks/wpindex.html). Detailed descriptions of Songda (2004) and Megi (2010) cases are similar to that in our previously study [*Sun et al*., 2015b], which are presented in the following two paragraphs.

Typhoon Songda (2004) is one of the most intense typhoons that made landfall on the main islands of Japan over the past 50 years. It resulted in extensive damages to Japan because of its strong winds and heavy rainfall. Songda originated near the Marshall Islands and developed into a tropical depression on 0600 UTC 26 August 2004 and quickly intensified when moving west-northwestward around the subtropical high over the WNP. Due to a break in the subtropical ridge, Songda turned northeastward toward western Japan on 6 September and made landfall on Nagasaki in western Kyushu Island in Japan at 0000 UTC 7 September (see Figure 1a).

Typhoon Megi (2010) is among the strongest TCs on record and the only supertyphoon of 2010. Megi originated over the WNP at around 11.9°N, 141.4°E and then developed into a tropical depression at 0000 UTC 13

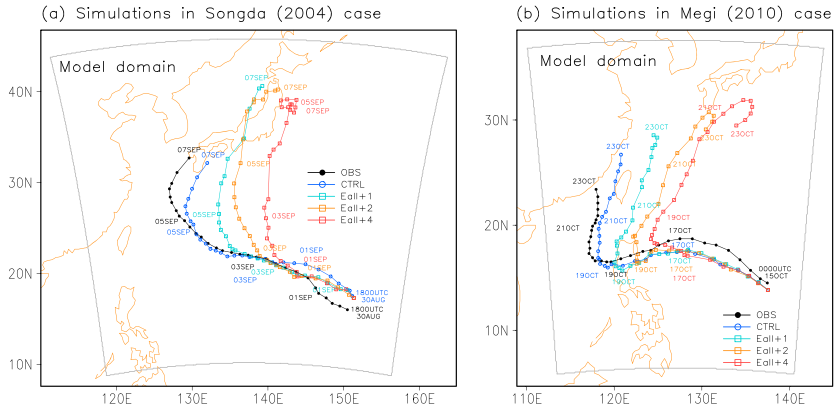

Figure 1. Storm track at 6 h intervals simulated in the sensitivity experiments with various underlying SST and the observed best TC track for (a) Songda (2004) and (b) Megi (2010).

October 2010. Because of the influence of the subtropical ridge and favorable environmental conditions, Megi started moving westward and then turned northwestward after its genesis and continued to intensify. Megi reached its lifetime peak intensity while making landfall over Isabela Province, Philippines, at 0325 UTC 18 October. It weakened when passing the Sierra Madre due to land effects but rapidly regained strength over the South China Sea. Later on 19 October, Megi turned northwestward and moved slowly due to the influence of the subtropical ridge, which significantly weakened in response to a deepening midlatitude shortwave trough that intruded into Southeast China. On October 23, Megi was downgraded to a tropical storm as it made landfall at Zhangpu in Fujian Province of China at 0455 UTC and further weakened to a tropical depression on October 23 (see Figure 1b).

The Weather and Forecasting Model version 3.3.1 (WRFV3.3.1) is used to simulate Songda (2004) and Megi (2010). The initial and boundary conditions of WRF are extracted from the 1° × 1° National Centers for Environmental Prediction (NCEP) Final Analysis (FNL, http://rda.ucar.edu/datasets/ds083.2/). The NCEP FNL product is produced by the Global Data Assimilation System, which continuously collects observational data from the Global Telecommunications System and other sources for analyses. The double-nested WRF model is run with grid spacings of 20 and 4 km, respectively. The inner domain, which is designed to define the storm, automatically moves following the position of the model storm via an automatic vortex-following algorithm [*Skamarock et al*., 2008]. There are 36 uneven σ levels in the vertical, extending from the surface to the model top at 50 hPa. Daily SST is updated using the NCEP FNL data. Note that the simulation periods and domains for the two cases are different. For the case of Songda, the outer domain is centered at 28°N, 137.5°E with 206 (north-south) × 222 (east-west) horizontal grid points, and the simulation starts at 0000 UTC 26 August and ends at 0600 UTC 07 September 2004 with a total of 294 h integration. For the case of Megi, the model domain is centered at 22°N, 122°E with 160 (north-south) × 180 (east-west) grid points, and the simulation is initialized at 0000 UTC 14 October and ends at 0000 UTC 24 October 2010, covering a total of 240 h. The outer domains of the two cases all extend far enough south to capture the recurvature of the TCs and the WPSH withdrawal/extension. Note that the inner domains start after 114 h and 24 h of model integration for the cases of Songda and Megi, respectively, when the storm entered the outer domain.

The Mellor-Yamada-Janjić boundary layer scheme [*Mellor and Yamada*, 1982; *Janjić*, 2002] and Monin-Obukhov surface layer scheme [*Monin and Obukhov*, 1954; *Webb*, 1970; *Beljaars*, 1994] are used in this study. Some other important physical schemes used here include the single-moment three-class *Hong et al*. [2004] and *Thompson et al*. [2004] microphysical schemes for the cases of Songda and Megi, respectively, and Kain-Fritsch cumulus parameterization scheme [*Kain and Fritsch*, 1990; *Kain*, 2004] for the two TC cases. More details about the model configuration can be found in the "namelist.input_Songda" and "namelist.input_Megi" files in supporting information Data Set S1. For each TC case, four experiments with different artificial SST increases are conducted to investigate the impact of ocean warming on TC track. In these experiments, the increases in the underlying SST in all domains are set to 0, 1, 2, and 4°C, respectively. For convenience, we define the four experiments as the CTRL one with 0°C SST increase, the Eall + 1 one with 1°C SST

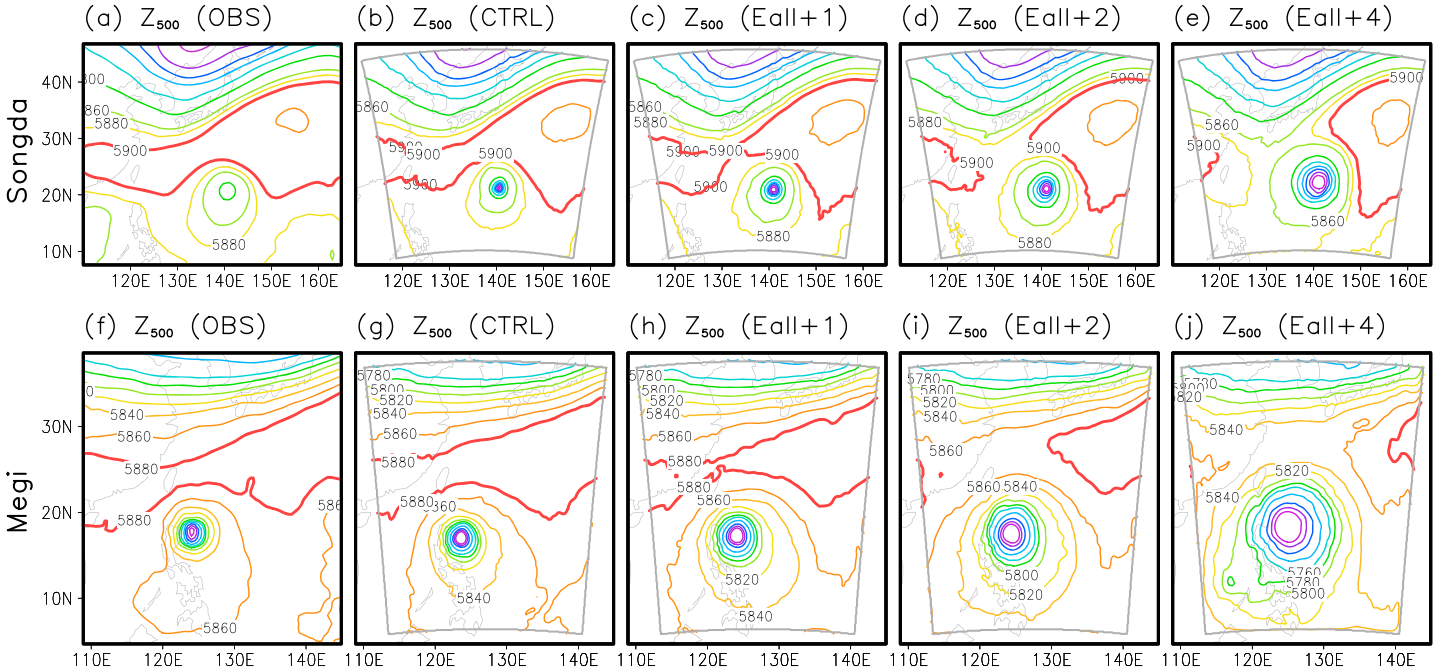

Figure 2. Geopotential height at 500 hPa (m) from NCEP reanalysis data and simulations at 0000 UTC 2 September 2004 and 0000 UTC 18 October 2010, corresponding to the cases of (a–e) Songda (2004) and (f–j) Megi (2010), respectively. The 5900 m contour is highlighted for the Songda case, and the 5880 m contour is highlighted for the Megi case.

increase, the Eall + 2 one with 2°C SST increase, and the Eall + 4 experiment with 4°C SST increase. All other model settings are the same in each of the four experiments.

3. Simulation Results

In an operational setting, the position of the storm center is calculated based on relevant variables (i.e., surface pressure and surface wind) in the inner domain with high resolution. Figure 1 compares the storm tracks simulated in the four SST experiments with the Joint Typhoon Warning Center best track of the cases of Songda and Megi. For each TC case, the CTRL experiment can well reproduce the TC track before and after its turning even after a lengthy simulation period. As the SST increase varies from 0 to 4°C, all four experiments yield a similar TC track during the first 4 days of the model integration; however, large differences in the simulated TC track appear after that point. Following the increase in SST, the simulated TC turns northward earlier, resulting in a poleward shift of the TC track, which is basically consistent with observations and simulation results in previous studies [*Kossin et al*., 2014; *Wu et al*., 2014; *Kossin et al*., 2016]. This result indicates that the simulated TC track is highly sensitive to the underlying SST, and the large-scale ocean warming can lead to a poleward shift of the TC even in a short period after the model initiation.

In the present study, as TCs are steered primarily by the large-scale environmental flow, the early northward turning of the TC can be attributed to the acceleration of a northward steering flow under ocean warming. The residual of the TC moving speed and the steering flow contribute little to the TC northward turning in the warmer SST experiments (see Figure S1). To further investigate the reasons for the acceleration of the northward steering flow and thus the northward turning of the TC under ocean warming, we depict the simulated 500 hPa geopotential height at the moment prior to the significant departure of the simulated TC position in the cases of Songda and Megi (Figure 2). A comparison of Figures 1 and 2 indicates that because of the strong influence of the large-scale steering flow on the southern edge of the WPSH, the time and location of the northward turning of the TCs are closely related to the degree of the weakening of the WPSH. Compared with that in CTRL, the TC's earlier turning simulated in the other three experiments with warmer SST (e.g., Eall + 1, Eall + 2, and Eall + 4) can be attributed to the weakening and thus splitting of the WPSH, as the simulated WPSH weakens and even breaks prior to the significant departure of the simulated TC track. This is because once the difference in the simulated TC position becomes significant,

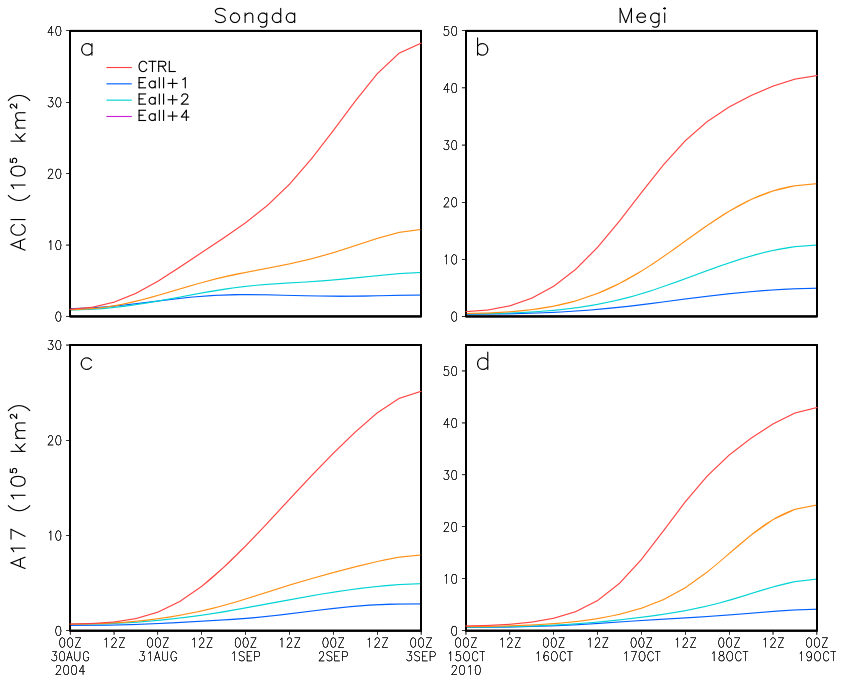

Figure 3. Temporal evolutions of ACI and A17 during specific periods in the SST sensitivity experiments for the (a and c) Songda case and (b and d) Megi case, respectively. The specific period is defined as the time period from 0000 UTC 30 August to 0000 UTC 3 September 2004 for Songda case and from 0000 UTC 15 October to 0000 UTC 19 October 2010 for Megi case.

as suggested by *Zhong* [2006], the TC at different positions may affect the intensity of the simulated WPSH near the TC at different degrees, which complicates the causal relationship between a TC's northward turning and WPSH weakening. For this reason, we focus on a specific time (i.e., from 0000 UTC 30 August to 0000 UTC 3 September 2004 for the Songda case and from 0000 UTC 15 October to 0000 UTC 19 October 2010 for the Megi case), when the difference in the simulated TC position is not significant enough to explain the involved mechanisms in the next section.

4. Physical Mechanism

4.1. Storm Size

As a warm core system, the WPSH is expected to intensify under ocean warming conditions if not considering the influences of other adjacent systems [*Pan and Oort*, 1983]. Thus, the decrease in the WPSH intensity in these sensitivity experiments with warmer SSTs should be attributed to changes in other adjacent systems associated with the ocean warming. In the present study, the TC is an important adjacent system to the WPSH; it expands significantly in terms of the outermost closed isobar as the SST increases (see Figure 2). The large difference in the storm size among these SST experiments further contributes to the difference in the simulated WPSH intensity and TC track as mentioned above.

In an operational setting, the storm size can be described as the area contained within the outermost closed isobar (ACI) at the surface, and the total storm area is where the 10 m sustained winds exceed tropical cyclone strength (>17 m s^{-1}) (A17) [*Sun et al*., 2015b; *Lau et al*., 2016]. For the cases of Songda and Megi in this study, the value of the outermost closed isobar is about 1000 hPa. Figure 3 illustrates the temporal evolutions of ACI and A17 in the two TC cases. Both ACI and A17 are highly sensitive to underlying SST and increase significantly following the SST increase. This is basically consistent with the model results of *Sun et al*. [2014a], which illustrate that a simulated TC under warmer SSTs is usually characterized by a larger inner core size and stronger winds outside the eyewall. The snapshots of the model-simulated radar reflectivity further illustrate the positive role of SST in determining the storm size, i.e., the simulated storm under warmer SST is accompanied by more active outer spiral rainbands, as suggested by *Wang* [2009], contributing to increases in the storm size (see Figure S2).

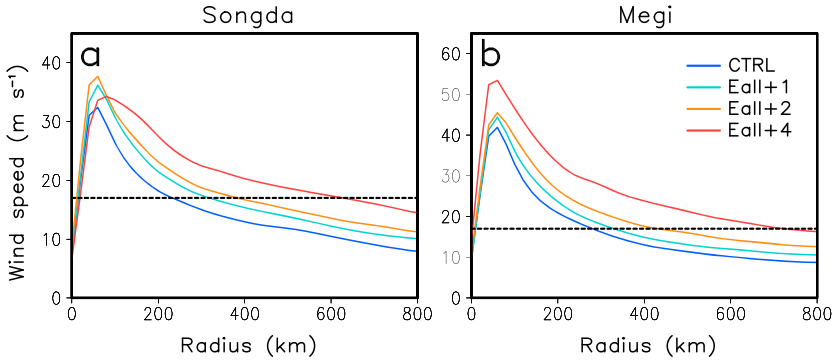

Figure 4. Tangential wind profiles at 10 m at 0000 UTC 2 September 2004 for the (a) Songda case and at 0000 UTC 18 October 2010 for the (b) Megi case, respectively. The black line represents the 17 m s^{-1} contour.

Theoretical and observational analyses indicate that storm size greatly impacts the motion of the storm [*Lester and Elsberry*, 1997, 2000; *Hill and Lackmann*, 2009; *Lee et al*., 2010]. Previous studies suggested that the storm size can affect storm motion over the WNP by influencing the extension/retraction of the WPSH and thus the large-scale environmental flow [*Sun et al*., 2015b] and by influencing the outer wind structure and thus the northward beta drift [*Hill and Lackmann*, 2009]. Despite the debate about which influence plays a more important role in the storm motion, the aforementioned studies all indicate that larger storms over the WNP are more likely to take a northward track. Based on the above discussion, the aforementioned earlier northward turning of the TC in the warmer SST experiments of the present study can be attributed to the larger TC size. In the following paragraphs, we will mainly focus on the process, whereby the SST affects the TC size, which eventually leads to the change in TC motion.

The storm size can be seen from the surface tangential wind profile, which not only determines the A17 but also reflects the ACI because the value of the tangential wind is closely related to the density of the isobars. Figure 4 illustrates the tangential wind profiles at 10 m in the aforementioned stage for the cases of Songda and Megi. As expected, the TC size, in terms of the radius of gale force wind (17 m s^{-1}), increases significantly with the increase in underlying SST. For convenience, we define the eye region and the eyewall region as the inner region, and the region outside the eyewall and within a radius of 300 km is defined as the outer region. The region outside the 300 km radius is defined as the remote region.

Generally, the tangential wind profile is determined by the storm intensity (i.e., the maximum wind speed, MWS), the storm inner core size (i.e., the radius of maximum wind, RMW), and the slope of tangential winds outside the RMW. According to the theoretical result of *Carr and Elsberry* [1997], the slope of the tangential winds outside the RMW is controlled by the Coriolis parameter *f*, which is determined by the latitude. This explains why the simulated slopes in the remote region are similar among these different SST experiments during the aforementioned period, as the difference in the simulated TC position is not significant during this period. However, for the outer region, following the increase in SST, the slope becomes somewhat different from that in CTRL, resulting in an additional increase in the outer tangential winds that are attributed to the increase in the outer surface enthalpy flux (SEF) associated with ocean warming. This argument will be further elaborated in sections 4.2 and 4.3. As the underlying SST increases, the increase in the simulated TC size can mainly be attributed to changes in the wind profiles in the inner and outer regions that are within 300 km radius from the TC center during the focus period of this study. Specifically, as shown in Figure 4, besides the additional increase in the outer tangential wind, the increases in MWS and RMW also play an important role in determining the expansion of the storm size as the SST increases. As it is straightforward to understand the increase in TC intensity (e.g., MWS) with a warmer ocean due to increased latent and sensible heat fluxes, we put more emphasis on the impact of SST on the TC inner core size (RMW) and outer winds and the mechanisms involved in the following paragraphs.

4.2. Sea Surface Entropy

Several previous studies indicated that the underlying SST affects TC activity (e.g., TC intensity and size) by supplying surface enthalpy flux (SEF) into the TC [*Emanuel*, 1986; *Rotunno and Emanuel*, 1987; *Xu and*

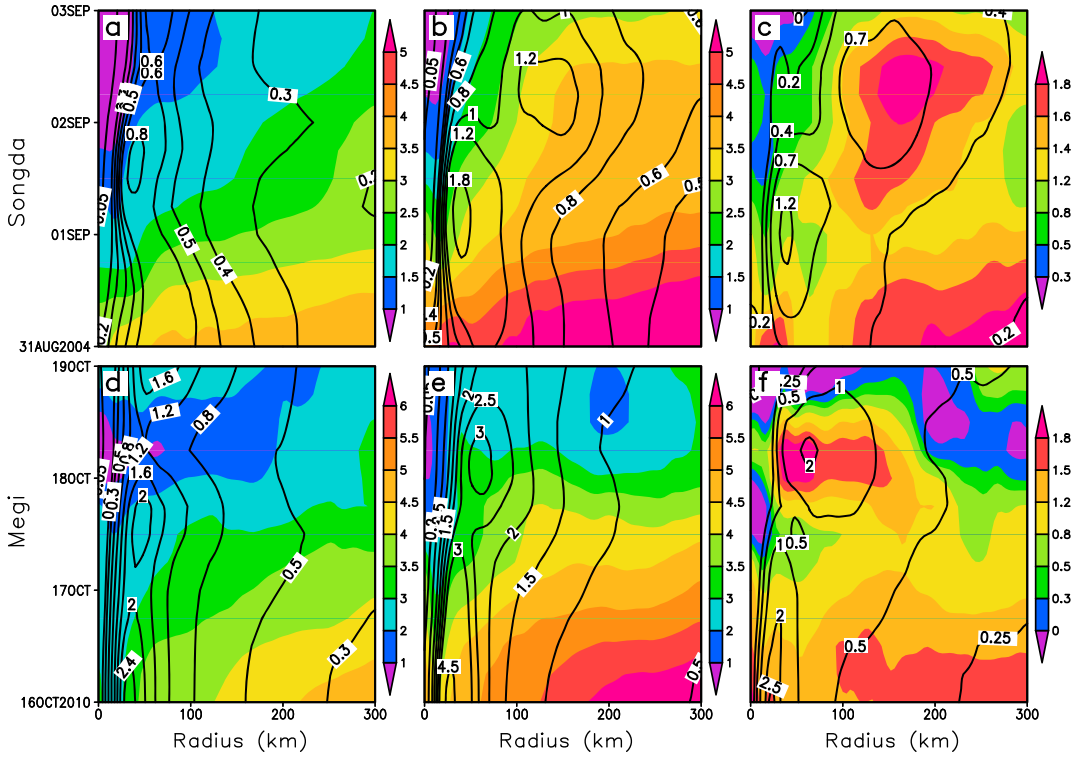

Figure 5. Hovmöller diagrams of azimuthally averaged ASMD (g kg^{-1}, shaded) and latent heat fluxes (10^3W m^{-2}, contoured) in (a and d) CTRL, (b and e) Eall + 2, and (c and f) their differences (Eall + 2 minus CTRL) for the cases of Songda (Figures 5a–5c) and Megi (Figures 5d–5f).

Wang, 2010]. SEF is a sum of the latent and sensible heat fluxes. The latent heat flux is determined by the surface wind speed and the air-sea moisture difference (ASMD), defined as the sea surface saturation specific humidity minus air specific humidity at 2 m; the sensible heat flux is determined by the surface wind speed and air-sea temperature difference, i.e., SST minus the air temperature at 2 m. As the latent heat flux is about 1 order of magnitude greater than the sensible heat flux (see Figures 5 and S3), the pattern (e.g., radial distribution) of latent heat flux is similar to that of SEF. Both patterns also have similar evolutions (see also Figure 6). Moreover, compared with the indirect impact of SST on surface wind speed, SST directly determines saturation specific humidity on the ocean surface and thus ASMD. Therefore, ASMD is key in understanding the responses of latent heat flux and thus SEF to SST change.

Figure 5 displays a Hovmöller diagram of the azimuthal-averaged ASMD and latent heat flux in CTRL, Eall + 2, and their differences for the cases of Songda and Megi. Following the increases in SST, the increased saturation-specific humidity results in increases in ASMD, which brings more latent heat flux into the TC eyewall, and eventually leads to a stronger TC (Figures 5a, 5b, 5d, and 5e). It is important to note that consistent with the results of *Sun et al.* [2013], as the low-level inflowing air approaches the eyewall, surface moisture gradually increases due to the moistening effect of the warmer SST in the TC outer region. As a result, the ASMD is relatively larger in the TC outer region (>80 km from the TC center) and relatively smaller in the TC inner region (≤80 km from the TC center), which further leads to an outward expansion of the area with latent heat flux increase (Figures 5c and 5f). As suggested by recent studies, changes in the radial distribution of SEF contribute greatly to changes in the tangential wind profile and thus the storm size [*Xu and Wang*, 2010; *Miyamoto and Takemi*, 2010; *Sun et al.*, 2013, 2014a]. Namely, the SEF in different regions plays different roles in determining the tangential wind profile, which will be elaborated in the following section.

4.3. Tangential Winds

To understand how the surface tangential winds (and thus the storm size) respond to changes in the underlying SEF that is associated with SST, we perform a momentum budget analysis. As suggested by *Xu*

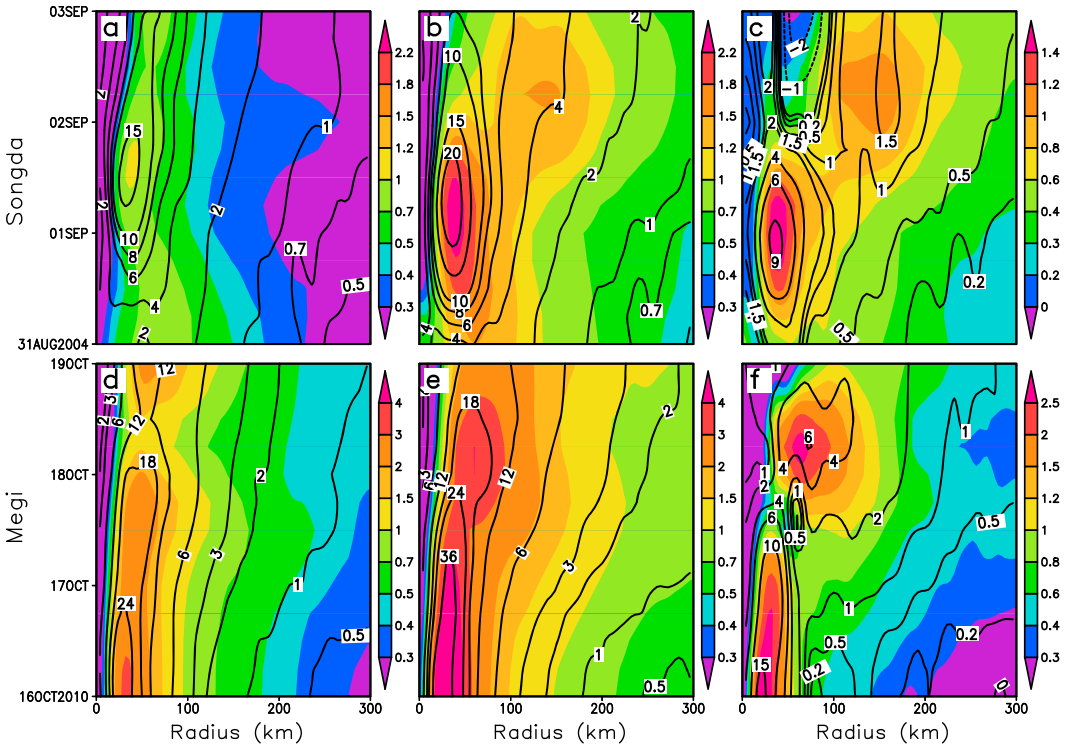

Figure 6. Hovmöller diagrams of azimuthally averaged SEF (10^3W m^{-2}, shaded) and radial sea level pressure gradient (10^{-2} Pa m^{-1}, contoured; inward is positive) in (a and d) CTRL, (b and e) Eall + 2, and (c and f) their differences (Eall + 2 minus CTRL) for the cases of Songda (Figures 6a–6c) and Megi (Figures 6d–6f).

and Wang [2010], the budget equations for the azimuthal mean radial and tangential winds can be approximated by

$$\frac{\mathrm{d}\overline{u}}{\mathrm{d}t} = -\frac{1}{\overline{\rho}}\frac{\partial \overline{p}}{\partial r} + \frac{\overline{V}^2}{r} + f\overline{V} + \overline{F}_u + \overline{D}_u, \tag{1}$$

and

$$\frac{\partial \overline{V}}{\partial t} = -\overline{u}\,\overline{\varsigma}_a + \overline{w}\frac{\partial \overline{V}}{\partial z} + \overline{F}_V - \overline{u'\varsigma'} - \overline{w'\frac{\partial V'}{\partial z}} + \overline{D}_V, \tag{2}$$

where t is time; z is height; r is the radius; f is the Coriolis parameter; $\overline{u}$, $\overline{V}$, and $\overline{w}$ are azimuthally averaged radial and tangential winds and vertical velocity; $\overline{\varsigma}_a$ is the azimuthally averaged vertical absolute vorticity; $\overline{\rho}$ and $\overline{p}$ are air density and pressure; u', V', w', and ς' are the deviations of radial, tangential, vertical winds, and vertical relative vorticity from their corresponding azimuthally averaged values, respectively; $\overline{F}_u$, $\overline{F}_V$, $\overline{D}_u$, and $\overline{D}_V$ are parameterized subgrid-scale vertical diffusions of radial and tangential winds (including surface fraction) and horizontal diffusions of radial and tangential winds, respectively. *Wang* [2009] and *Xu and Wang* [2010] indicated that it is the change in the pressure gradient force ($-\frac{1}{\overline{\rho}}\frac{\partial \overline{p}}{\partial r}$ term) that leads to the gradient wind imbalance ($\frac{\mathrm{d}\overline{u}}{\mathrm{d}t}$ term) and thus the changes in the low-level inflow, which further affect the radial distribution of tangential winds through $-\overline{u}\,\overline{\varsigma}_a$. Note that the changes in pressure gradient are associated with the hydrostatic adjustment to diabatic heating in convection that is closely related to changes in the SEF.

In the present study, the momentum budget is calculated at the surface level to investigate the impact of SEF on the surface radial and tangential winds. Figure 6 displays a Hovmöller diagram of the azimuthal mean SEF and radial pressure gradient in CTRL and Eall + 2 and their differences for the cases of Songda and Megi. As expected, due to more energy exchanges at the air-sea interface (i.e., SEF), the warmer-SST experiment (e.g., Eall + 2) produces a larger magnitude of latent heating, which results in a larger-pressure decrease and thus a

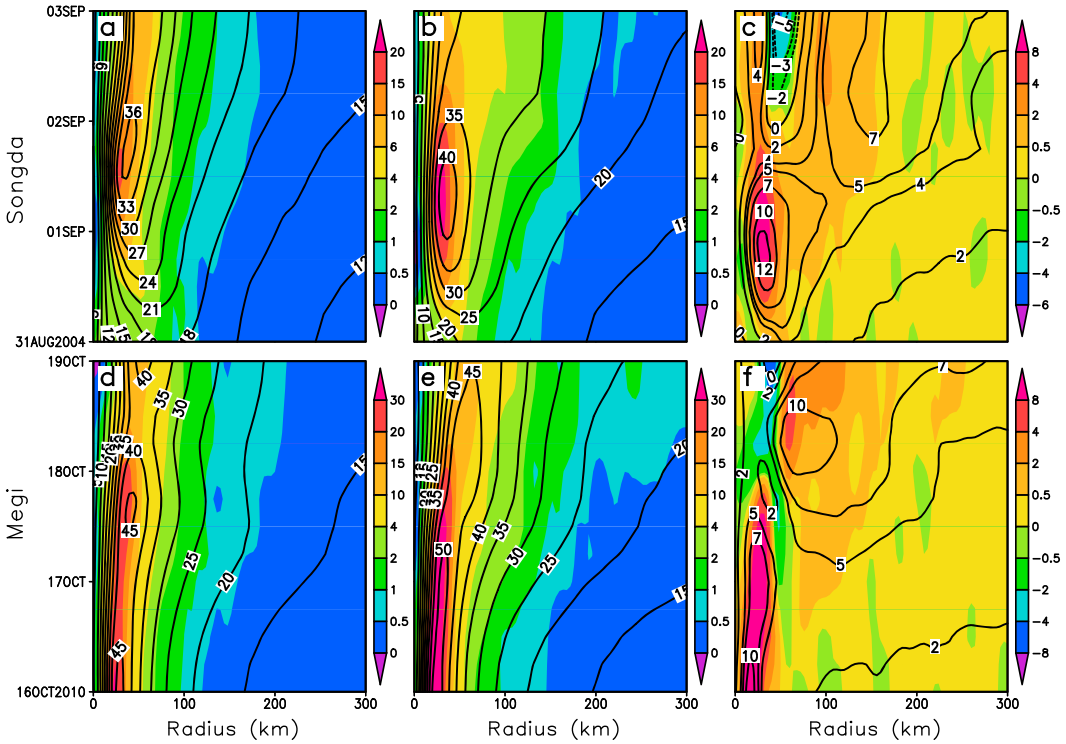

Figure 7. Hovmöller diagrams of azimuthally averaged absolute vorticity ($\overline{\varsigma}_a$, 10^{-3} s^{-1}, shaded) and its radial advection ($-\overline{u}\overline{\varsigma}_a$, 10^{-2} m s^{-2}, contoured) at 10 m in (a and d) CTRL, (b and e) Eall + 2, and (c and f) their differences (Eall + 2 minus CTRL) for the cases of Songda (Figures 7a–7c) and Megi (Figures 7d–7f).

larger radial pressure gradient, especially in the eyewall (see also Figure S4). More importantly, compared with that in CTRL, the increase in SEF and thus the increase in the radial pressure gradient in Eall + 2 are still mainly concentrated near the eyewall within a radius of about 50 km from TC center during the initial stage (before 0000 UTC 1 September 2004 for the Songda case and 1200 UTC 16 October 2010 for the Megi case) due to strong surface winds in the TC eyewall (see also Figure S5). Meanwhile, the outer SEF and radial pressure gradient outside the eyewall increase significantly with time, and their growth rates are much larger than those in the eyewall due to the larger ASMD outside the eyewall (Figures 5c, 5f, 6c, and 6f). This leads to outward expansion of the SEF and radial sea level pressure gradient. Note that the impact of SEF on the radial pressure gradient is not limited to the surface level; its influence can extend to the height of the boundary layer containing the low-level inflow (see Figure S4), which is consistent with the model results in *Sun et al*. [2014a] (see their Figure 8). This facilitates the growth of the outer inward radial winds within the boundary layer under the joint effect of the radial forcing term excluding the diffusion in equation (1) (Figures S6 and S7). The accelerated outer inward winds are favorable for the growth of outer tangential winds, which in turn increases the outer SEF and further enhances outer tangential winds after the initial stage.

Figure 7 shows Hovmöller diagrams of the azimuthally averaged absolute vorticity ($\overline{\varsigma}_a$) and its radial advection ($-\overline{u}\,\overline{\varsigma}_a$) in CTRL and Eall + 2 and their differences for the cases of Songda and Megi. Compared with that in CTRL, the absolute vorticity in Eall + 2 is remarkably larger not only in the eyewall region but also in the outer region. This is because warmer SST can induce larger outer diabatic heating and thus more active outer spiral rainbands (see Figures S2 and S4) by supporting more SEF (see Figure 6), which leads to the increase in outer vorticity as suggested by *Xu and Wang* [2010]. The increased absolute vorticity outside the eyewall, in combination with the enhanced low-level inflow outside the eyewall, increases the tangential wind speed outside the RMW through $-\overline{u}\overline{\varsigma}_a$ (see also Figure S5). The increased tangential wind, in turn, leads to an increase in the SEF over the outer region. This is a positive feedback that dominates the further enhancement of the outer tangential winds and the expansion of the RMW. The RMW expansion results in a smaller centrifugal force and induces a subgradient wind, preventing further expansion of the RMW. This is a

major mechanism for the increase in the RMW and the aforementioned additional increase in outer tangential winds in Eall + 2. Together with the increase in MWS, the increase in the RMW and the additional increase in the outer tangential winds all contribute greatly to the increase in TC size, which eventually leads to the weakening of the WPSH and the early northward turning of the TC in Eall + 2. In addition, comparing the results in the other warmer SST experiments (e.g., Eall + 1 and Eall + 4) with that in CTRL, we reach similar conclusions (figures omitted).

4.4. Validation of the Effect of Ocean Warming on Storm Track

The two cases, i.e., Songda (2004) and Megi (2010), used in the present study are both supertyphoons. To investigate whether our main conclusions are also valid for weak TCs, we have examined two additional TC cases over the WNP, i.e., Mirinae (2009) and Omais (2010). Compared with those of Songda (2004) and Megi (2010), the maximum intensities of Mirinae (2009) and Omais (2010) are much weaker. Moreover, the two cases are different in track pattern and duration. Mirinae (2009) is characterized by a westward moving track and relatively long duration, while Omais (2010) is characterized by a northwestward moving track and relatively short duration. Similar to the model configurations for Songda (2004) and Megi (2010), the model domains of the two extra TC cases are all doubly nested with grid spacings of 20 km and 4 km, respectively. The inner domain moves automatically to follow the position of the model storm via an automatic vortex-following algorithm [*Skamarock et al*., 2008]. For the case of Mirinae, the outer domain is centered at 20°N, 130°E with 200 (north-south) × 300 (east-west) horizontal grid points. For the case of Omais, the model domain is centered at 10°N, 135°E with 201 (north-south) × 250 (east-west) grid points. Details about the model configuration can be found in the "namelist.input_Mirinae" and "namelist.input_Omais" files in supporting information Data Set S2. For each TC case, four experiments with different SST increases (i.e., CTRL, Eall + 1, Eall + 2, and Eall + 4) are conducted to investigate the impact of ocean warming on TC track.

For each TC case, the CTRL experiment can well reproduce the TC track (see Figure S6). However, the sensitivity of TC track to ocean warming is notably different between the Mirinae case and the Omais case (see Figure S6). For the Mirinae case, as the SST increase varies from 0 to 4°C, all four experiments yield a similar TC track during the first 4 days of model integration, but large differences in TC track occur after that point. Following the increase in SST, the simulated TC turns northward due to the weakening and thus splitting of the WPSH (see Figure S7a), resulting in a poleward shift of the TC track. For the Omais case, in warmer SST experiments, the simulated TC recurves more significantly, resulting in an earlier northward turning of the TC. Note that there is only a slight difference in TC track simulations among the SST sensitivity experiments, which may be attributed to the short TC duration and weak WPSH (see Figure S7b). Specifically, the short TC duration makes its impact on the WPSH intensity quite limited, while the weak WPSH implies a weak WPSH-related large-scale forcing. Under the joint effects of short TC duration and weak WPSH intensity, the feedback of TC on the WPSH intensity and thus TC track is limited. As a result, for the Omais case, the simulated TC track changes little with the increase in SST in spite of the SST impact on TC intensity and size. Therefore, for the cases of Mirinae and Omais, the SST increase contributes more or less to the change in TC track, namely, the simulated TC track turns northward earlier following the increase in SST. This is basically consistent with the results of the case studies for Songda and Megi.

To further validate our major conclusions of the effect of ocean warming on storm size and thus the WPSH and storm motion, we have conducted three additional SST sensitivity experiments with 0, 1 and 2°C of SST increase (CTRL, Eall + 1, and Eall + 2), respectively. Each experiment covers the peak of the typhoon season (from 1 May to 1 November) over a 10 year period (2001–2010) in the western North Pacific (100° to 180°E, 0° to 60°N). The model is run at 20 km horizontal resolution. Three climate simulations with the same atmospheric initial and lateral boundary conditions but different SSTs are carried out. In the CTRL experiments, SST remains unchanged from that in the NCEP FNL data; in the Eall + 1 and Eall + 2 experiments, the increases in SST are homogeneously set to 1°C and 2°C over the entire model domain, respectively. More details about the model configuration can be found in the "namelist.input_climate" files in supporting information Data Set S3. The criteria for identifying TCs are provided in the supporting information vortex criteria. Note that the interaction between TCs over the South China Sea and the WPSH is substantially different to that between TCs over other regions in the WNP and the WPSH. For this reason, we only consider TCs over certain regions in the WNP excluding the South China Sea.

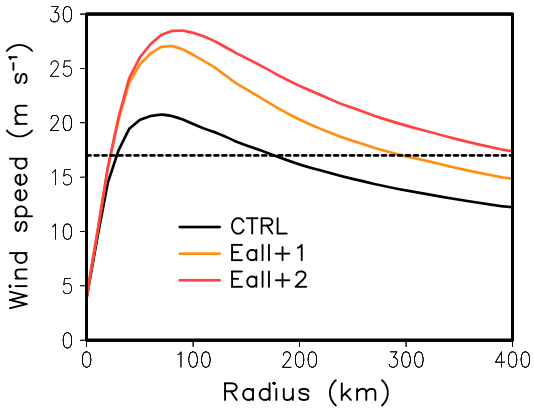

Figure 8. Tangential wind profiles at 10 m averaged during the TC mature stage over the WNP for the three sensitivity experiments. The mature TC stage is defined as the period when the maximum wind speed at 10 m (V_{max}) is close to its lifetime maximum wind speed at 10 m ($V_{life\text{-}max}$), i.e., $|V_{max} - V_{life\text{-}max}| \leq 3$ m s^{-1}.

In this study, as the underlying SST increases, the calculated MWS also increases significantly, while the RMW expands, leading to an additional increase in outer wind strength (Figure 8). As a result, the calculated storm size, in terms of radius of gale force wind, increases significantly following the increases in SST over the WNP. This is basically similar to the results of the case studies of Songda and Megi, which also show an expansion of TC size under ocean warming. Moreover, consistent with the aforementioned impact of ocean warming, with the increase in TC size, the main body of the WPSH withdraws eastward (Figure 9). Due to the strong steering effect of the WPSH-related large-scale environmental flow, the climatological TC track (in terms of the averaged positions where TCs start, reach their lifetime maximum intensity, and end) basically is along the edge of the WPSH. Following the increase in underlying SST, the simulated TCs tend to turn from northwestward to northeastward over the WNP (Figure 9), which is consistent with the results of case studies for Songda and Megi investigated in detail here (see Figure 1). The results of these climate simulations provide further evidences to support the aforementioned impacts of ocean warming on storm size and thus the WPSH and TC track over the WNP. This also implies that the TC threat to East Asian countries may be reduced due to changes in TC track, assuming that the ocean warming trend continues in the future.

5. Conclusions and Discussion

In this study, the sensitivity of TC track over the WNP to SST changes has been investigated through several suites of sensitivity experiments using the high-resolution WRF model. Since many previous studies have elaborated the impact of storm size on the WPSH intensity and thus the storm motion, we put more emphasis on the physical processes involved in the ocean warming influences on the storm size. Results of our Songda (2004) and Megi (2010) case studies indicate that as the underlying SST increases, the tangential wind profile changes substantially, resulting in a significant increase in TC size, which eventually leads to the eastward withdrawal of the WPSH and the northward turning of TCs over the WNP. In addition, besides SST, the ocean heat content is also an important factor which is particularly important for TC intensification or weakening when the TC moves at slow speed. For TCs with near average translation speeds, this effect might be limited.

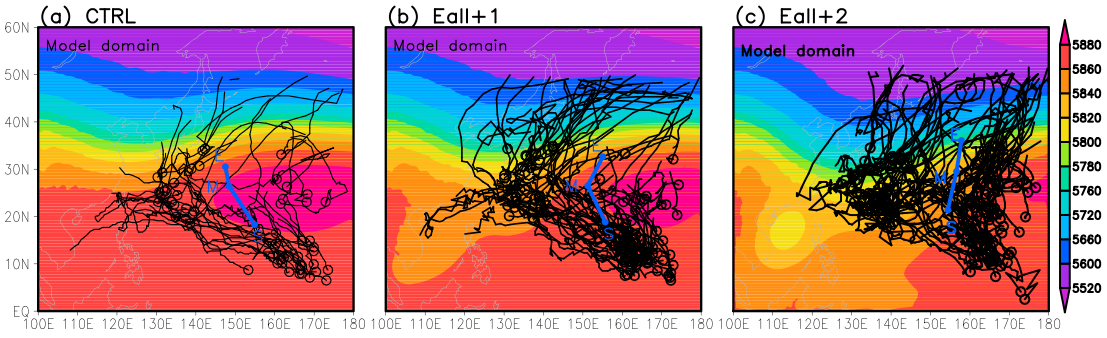

Figure 9. (a–c) Simulated 500 hPa geopotential height (m, shaded) averaged over the simulation period and simulated storm tracks (black lines) over the WNP in the three sensitivity experiments. The blue dots near the blue characters of "S," "M," and "E" represent the averaged positions where storms start, reach their lifetime maximum intensity and end, respectively. These blue dots are linked with blue lines.

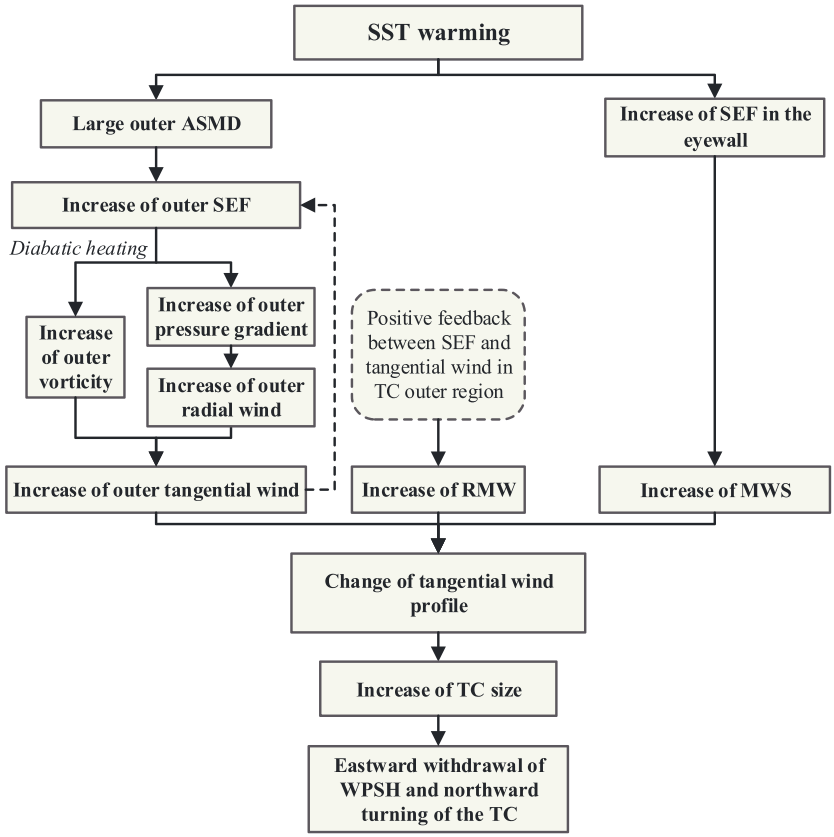

Figure 10. Schematic diagram summarizing the possible mechanisms responsible for the impact of SST on TC track over the WNP.

The study of the effect of ocean heat content on TCs requires long-term simulations of coupled ocean-atmosphere models. To a first-order approximation, we simply neglect this effect in the current study and focus on investigating the effects of increasing SST on TC size and track.

The mechanisms for the SST impact on TC size and TC track are discussed systematically from the perspectives of SEF and the TC tangential wind profile. Unlike many previous studies that focused on the impact of SST on TC intensity, we pay more attention to the impact of SST on TC outer winds. The results are schematically summarized in Figure 10. As the underlying SST increases, the increase in ASMD is relatively larger in the outer region than in the inner region, which leads to a larger growth rate of the SEF in the outer region than in the inner region. The outer diabatic heating associated with the increased outer SEF has two effects. On the one hand, it causes an increase in the vorticity over the outer region; on the other hand, it leads to increases in the outer pressure gradient and thus outer radial winds. According to equation (2), the above two effects both contribute to the increase in tangential wind speed through $-\overline{u}\overline{\varsigma}_a$. The increased tangential wind, in turn, leads to further increases in SEF in the outer region. The positive feedback between the SEF and tangential winds results in further growth of outer tangential winds and thus the increase in RMW. Together with the increase in MWS caused by warmer SST and thus larger SEF near the eyewall, the increase in RMW and the additional increase in tangential wind all contribute to the change in the tangential wind profile and result in the expansion of the TC size in terms of the radius of gale force wind (17 m s^{-1}). As suggested in a recent study [*Sun et al.*, 2015b], the increase in TC size can eventually lead to the withdrawal of the WPSH and thus the northward turning of the TC. In addition, the results of the additional climate simulations provide further evidences to support the aforementioned conclusions of ocean warming impact on TC size and thus the WPSH and TC track over the WNP.

In this study, we focus on the physical mechanism for SST impact on TC size. Details on the impact of TC size on the WPSH and TC track can be referred to our previously published paper [*Sun et al.*, 2015b], which elaborates the mechanisms on how the storm size affects the WPSH intensity and TC motion, especially the

dynamic interaction between the TC and WPSH. In addition, it is important to note that in the present study, we only consider the TC track over certain regions in the WNP excluding the South China Sea. The involved physical mechanisms cannot explain all the TC tracks. TCs over the South China Sea, for example, show no significant poleward shift trend under the ocean warming condition (figure omitted), which may be attributed to the weak interaction between these TCs and the WPSH due to the long distance between them. More TC case studies are needed to answer the question whether the aforementioned mechanisms can be applied to TCs over other ocean basins of the world.

Due to the inherent limitation of the numerical model used in the present study, simulated TC activities (e.g., TC intensity, structure, and track) differ from observations to varying degrees. The model results are considered to be highly uncertain in each experiment. However, the trends in TC activity with changing SSTs are much less uncertain based on the comparison results of the SST sensitivity experiments, as the simulated trends are less sensitive to possible biases in the model results. Moreover, the physical mechanisms revealed in this study not only help us better understand the impact of SST on TC size and thus TC track over the WNP but also shed some light on the possible change in TC track over the WNP under global warming in the future. Our results imply that the threat of typhoons to East Asian countries may be reduced due to the poleward shift of TCs, assuming that ocean warming continues in the future. This is consistent with results of previous studies [*Wu and Wang*, 2004; *Bengtsson et al*., 2006; *Kossin et al*., 2014, 2016]. Note that the results of the semiidealized numerical experiments in the present study only provide a necessary condition but are still far from sufficient for understanding the impact of global warming on TC tracks. This is because, on one hand, the changes in the large-scale circulation under global warming have not been considered in the model design of SST sensitivity experiments; on the other hand, SST may not change in a uniform pattern in the future. Impacts of SST changes at different magnitudes and in different spatial patterns will be studied in our future research.

Acknowledgments
Data supporting the model configurations for the two TC-case simulations, the two additional weak TC-case simulations, and climate simulations are available as supporting information Data Sets S1–S3. This work is sponsored by National Key Research Project 2017YFA0603802, China NSF grant 41430426, 973 project 2015CB453200, China NSF grant 41605072, Jiangsu projects BK20160768 and BK20150062, and Jiangsu Shuang-Chuang Team (R2014SCT001). This is SOEST publication number 10215, IPRC publication number 1284, and ESMC publication number 176.

References

Beljaars, A. C. M. (1994), The parameterization of surface fluxes in large-scale models under free convection, *Q. J. R. Meteorol. Soc.*, *121*, 255–270, doi:10.1002/qj.49712152203.

Bell, M. M., and M. T. Montgomery (2008), Observed structure, evolution, and potential intensity of category 5 Hurricane Isabel from 12 to 14 September, *Mon. Weather Rev.*, *136*, 2023–2046, doi:10.1175/2007MWR1858.1.

Bengtsson, L., K. I. Hodges, and E. Roeckner (2006), Storm tracks and climate change, *J. Clim.*, *19*, 3518–3543.

Carr, L. E., III, and R. L. Elsberry (1997), Models of tropical cyclone wind distribution and beta-effect propagation for application to tropical cyclone track forecasting, *Mon. Weather Rev.*, *125*, 3190–3209, doi:10.1175/1520-0493(1997)125<3190:MOTCWD>2.0.CO;2.

Cox, P. M., R. A. Betts, C. D. Jones, S. A. Spall, and I. J. Totterdell (2000), Acceleration of global warming due to carbon-cycle feedbacks in a coupled climate model, *Nature*, *408*, 184–187, doi:10.1038/35041539.

Elsner, J. B., J. C. Trepanier, S. E. Strazzo, and T. H. Jagger (2012), Sensitivity of limiting hurricane intensity to ocean warmth, *Geophys. Res. Lett.*, *39*, L17702, doi:10.1029/2012GL053002.

Emanuel, K. A. (1986), An air-sea interaction theory for tropical cyclone: Part I: Steady state maintenance, *J. Atmos. Sci.*, *43*, 585–604, doi:10.1175/1520-0469(1986)043<0585:AASITF>2.0.CO;2.

Fiorino, M., and R. L. Elsberry (1989), Some aspects of vortex structure related to tropical cyclone motion, *J. Atmos. Sci.*, *46*, 975–990, doi:10.1175/1520-0469(1989)046<0975:SAOVSR>2.0.CO;2.

George, J. E., and W. M. Gray (1977), Tropical cyclone recurvature and nonrecurvature as related to surrounding wind-height fields, *J. Appl. Meteorol.*, *16*, 34–42.

Hill, K. A., and G. M. Lackmann (2009), Influence of environmental humidity on tropical cyclone size, *Mon. Weather Rev.*, *137*, 3294–3315, doi:10.1175/2009MWR2679.1.

Holland, G. J. (1983), Tropical cyclone motion: Environmental interaction plus a beta effect, *J. Atmos. Sci.*, *40*, 328–342, doi:10.1175/1520-0469(1983)040<0328:TCMEIP>2.0.CO;2.

Holland, G. J. (1997), The maximum potential intensity of tropical cyclones, *J. Atmos. Sci.*, *54*, 2519–2541, doi:10.1175/1520-0469(1997)054<2519:TMPIOT>2.0.CO;2.

Hong, S.-Y., J. Dudhia, and S.-H. Chen (2004), A revised approach to ice microphysical processes for the bulk parameterization of clouds and precipitation, *Mon. Weather Rev.*, *132*, 103–120, doi:10.1175/1520-0493(2004)132<0103:ARATIM>2.0.CO;2.

Janjić, Z. I. (2002), Nonsingular implementation of the Mellor-Yamada level 2.5 scheme in the NCEP Meso model, NCEP Off. Note 437, 61 pp.

Kain, J. S. (2004), The Kain-Fritsch convective parameterization: An update, *J. Appl. Meteorol.*, *43*, 170–181, doi:10.1175/1520-0450(2004)043<0170:TKCPAU>2.0.CO;2.

Kain, J. S., and J. M. Fritsch (1990), A one-dimensional entraining/detraining plume model and its application in convective parameterization, *J. Atmos. Sci.*, *47*, 2784–2802, doi:10.1175/1520-0469(1990)047<2784:AODEPM>2.0.CO;2.

Kang, N.-Y., and J. B. Elsner (2012), Consensus on climate trends in western North Pacific tropical cyclones, *J. Clim.*, *25*, 7564–7573, doi:10.1175/JCLI-D-11-00735.1.

Kang, N.-Y., and J. B. Elsner (2016), Climate mechanism for stronger typhoons in a warmer world, *J. Clim.*, *29*, 1051–1057, doi:10.1175/JCLI-D-15-0585.1.

Knutson, T. R., J. L. McBride, J. Chan, K. Emanuel, G. Holland, C. Landsea, I. Held, J. P. Kossin, A. K. Srivastava, and M. Sugi (2010), Tropical cyclones and climate change, *Nat. Geosci.*, *3*, 157–163.

Kossin, J. P., K. A. Emanuel, and G. A. Vecchi (2014), The poleward migration of the location of tropical cyclone maximum intensity, *Nature*, *509*, 349–352.

Kossin, J. P., K. A. Emanuel, and S. J. Camargo (2016), Past and projected changes in western North Pacific tropical cyclone exposure, *J. Clim.*, *29*, 5725–5739.
Lau, K.-M., and H. Weng (1999), Interannual, decadal-interdecadal, and global warming signals in sea surface temperature during 1955-97, *J. Clim.*, *12*, 1257–1267.
Lau, K.-M., J. J. Shi, W. K. Tao, and K. M. Kim (2016), What would happen to superstorm Sandy under the influence of a substantially warmer Atlantic Ocean?, *Geophys. Res. Lett.*, *43*, 802–811, doi:10.1002/2015GL067050.
Lee, C.-S., K. K. W. Cheung, W.-T. Fang, and R. L. Elsberry (2010), Initial maintenance of tropical cyclone size in the western North Pacific, *Mon. Weather Rev.*, *138*, 3207–3223, doi:10.1175/2010MWR3023.1.
Lee, T.-C., T. R. Knutson, H. Kamahori, and M. Ying (2012), Impacts of climate change on tropical cyclones in the western North Pacific basin. Part I: Past observations, *Trop. Cyclone Res. Rev.*, *1*, 213–230.
Lester, E. C., III, and R. L. Elsberry (1997), Models of tropical cyclone wind distribution and beta-effect propagation for application to tropical cyclone track forecasting, *Mon. Weather Rev.*, *125*, 3190–3209, doi:10.1175/1520-0493(1997)125<3190:MOTCWD>2.0.CO;2.
Lester, E. C., III, and R. L. Elsberry (2000), Dynamical tropical cyclone track forecast errors. Part I: Tropical region error sources, *Weather Forecast.*, *15*, 641–661, doi:10.1175/1520-0434(2000)015<0641:DTCTFE>2.0.CO;2.
Maue, R. N. (2011), Recent historically low global tropical cyclone activity, *Geophys. Res. Lett.*, *38*, L14803, doi:10.1029/2011GL047711.
Mellor, G. L., and T. Yamada (1982), Development of a turbulence closure model for geophysical fluid problems, *Rev. Geophys. Space Phys.*, *20*, 851–875, doi:10.1029/RG020i004p00851.
Miyamoto, Y., and T. Takemi (2010), An effective radius of the sea surface enthalpy flux for the maintenance of a tropical cyclone, *Atmos. Sci. Lett.*, *11*, 278–282, doi:10.1002/asl.292.
Monin, A. S., and M. A. Obukhov (1954), Basic laws of turbulent mixing in the ground layer of the atmosphere, *Tr. Geofiz. Inst. Akad. Nauk. SSSR*, *151*, 163–187.
Pan, Y. H., and A. H. Oort (1983), Global climate variations connected with sea surface temperature anomalies in the eastern equatorial Pacific Ocean for the 1958–73 period, *Mon. Weather Rev.*, *111*, 1244–1258.
Persing, J., and M. T. Montgomery (2005), Is environmental CAPE important in the determination of maximum possible hurricane intensity?, *J. Atmos. Sci.*, *62*, 542–550, doi:10.1175/JAS-3370.1.
Rotunno, R., and K. A. Emanuel (1987), An air–sea interaction theory for tropical cyclones. Part II: Evolutionary study using a nonhydrostatic axisymmetric numerical model, *J. Atmos. Sci.*, *44*, 542–561, doi:10.1175/1520-0469(1987)044<0542:AAITFT>2.0.CO;2.
Skamarock, W. C., J. B. Klemp, J. Dudhia, D. O. Gill, D. M. Barker, M. G. Duda, X. Y. Huang, W. Wang, and J. G. Powers (2008), A description of the advanced research WRF version 3, *NCAR Tech. Note NCAR/TN-475+STR*, 113 pp. [Available at http://www.mmm.ucar.edu/people/skamarock/.]
Strazzo, S., J. B. Elsner, J. C. Trepanier, and K. A. Emanuel (2013), Frequency, intensity, and sensitivity to sea surface temperature of North Atlantic tropical cyclones in best-track and simulated data, *J. Adv. Model. Earth Syst.*, *5*, 500–509, doi:10.1002/jame.20036.
Strazzo, S. E., J. B. Elsner, and T. E. Larow (2015), Quantifying the sensitivity of maximum, limiting, and potential tropical cyclone intensity to SST: Observations versus the FSU/COAPS global climate model, *J. Adv. Model. Earth Syst.*, *7*, 586–599, doi:10.1002/2015MS000432.
Sun, Y., Z. Zhong, Y. Ha, Y. Wang, and X. D. Wang (2013), The dynamic and thermodynamic perspectives of relative and absolute sea surface temperature on tropical cyclone intensity, *Acta. Meteor. Sin.*, *27*, 40–49, doi:10.1007/s13351-013-0105-z.
Sun, Y., Z. Zhong, W. Lu, and Y. Hu (2014a), Why are tropical cyclone tracks over the western North Pacific sensitive to the cumulus parameterization scheme in regional climate modeling? A case study for Megi (2010), *Mon. Weather Rev.*, *142*, 1240–1249, doi:10.1175/MWR-D-13-00232.1.
Sun, Y., Z. Zhong, L. Yi, Y. Ha, and Y. Sun (2014b), The opposite effects of inner and outer sea surface temperature on tropical cyclone intensity, *J. Geophys. Res. Atmos.*, *119*, 2193–2208, doi:10.1002/2013JD021354.
Sun, Y., Z. Zhong, H. Dong, J. Shi, and Y. Hu (2015a), Sensitivity of tropical cyclone track simulation over the western North Pacific to different heating/drying rates in the Betts–Miller–Janjić scheme, *Mon. Weather Rev.*, *143*, 3478–3494, doi:10.1175/MWR-D-14-00340.1.
Sun, Y., Z. Zhong, L. Yi, T. Li, M. Chen, H. Wan, Y. Wang, and K. Zhong (2015b), Dependence of the relationship between the tropical cyclone track and western Pacific subtropical high intensity on initial storm size: A numerical investigation, *J. Geophys. Res. Atmos.*, *120*, 11,451–11,467, doi:10.1002/2015JD023716.
Thompson, G., R. M. Rasmussen, and K. Manning (2004), Explicit forecasts of winter precipitation using an improved bulk microphysics scheme. Part I: Description and sensitivity analysis, *Mon. Weather Rev.*, *132*, 519–542, doi:10.1175/1520-0493(2004)132,0519:EFOWPU.2.0.CO;2.
Vecchi, G. A., and B. J. Soden (2007), Effect of remote sea surface temperature change on tropical cyclone potential intensity, *Nature*, *450*, 1066–1070, doi:10.1038/nature06423.
Vecchi, G. A., K. L. Swanson, and B. J. Soden (2008), Whither hurricane activity?, *Science*, *322*, 687–689, doi:10.1126/science.1164396.
Wang, R., L. Wu, and C. Wang (2011), Typhoon track changes associated with global warming, *J. Clim.*, *24*, 3748–3752.
Wang, Y. (2009), How do outer spiral rainbands affect tropical cyclone structure and intensity?, *J. Atmos. Sci.*, *66*, 1250–1273.
Webb, E. K. (1970), Profile relationships: The log-linear range, and extension to strong stability, *Q. J. R. Meteorol. Soc.*, *96*, 67–90, doi:10.1002/qj.49709640708.
Webster, P. J., G. J. Holland, J. A. Curry, and H.-R. Change (2005), Changes in tropical cyclone number, duration, and intensity in a warming environment, *Science*, *309*, 1844–1846.
Wu, L., and B. Wang (2004), Assessing impacts of global warming on tropical cyclone tracks, *J. Clim.*, *17*, 1686–1698.
Wu, L., C. Chou, C.-T. Chen, R. Huang, T. R. Knutson, J. J. Sirutis, S. T. Garner, C. Kerr, C.-J. Lee, and Y.-C. Feng (2014), Simulations of the present and late-twenty-first-century western North Pacific tropical cyclone activity using a regional model, *J. Clim.*, *27*, 3405–3424.
Xu, J., and Y. Wang (2010), Sensitivity of tropical cyclone inner-core size and intensity to the radial distribution of surface entropy flux, *J. Atmos. Sci.*, *67*, 1831–1852, doi:10.1175/2010JAS3387.1.
Zhong, Z. (2006), A possible cause of a regional climate model's failure in simulating the east Asian summer monsoon, *Geophys. Res. Lett.*, *33*, L24707, doi:10.1029/2006GL027654.